Acta Pharmacologica Sinica 2017: 1486–1500
 1671-4083/17
www.nature.com/aps

Original Article

The novel resveratrol derivative 3,5-diethoxy-3′,4′-dihydroxy-*trans*-stilbene induces mitochondrial ROS-mediated ER stress and cell death in human hepatoma cells *in vitro*

Jae-woo PARK[1, #], Woo-gyun CHOI[1, #], Phil-jun LEE[2], Su-wol CHUNG[1], Byung-sam KIM[1], Hun-taeg CHUNG[1], Sungchan CHO[3], Jong-heon KIM[4], Byoung-heon KANG[5], Hyoungsu KIM[2], Hong-pyo KIM[2], Sung-hoon BACK[1, *]

[1]School of Biological Sciences, University of Ulsan, Ulsan 44610, Korea; [2]School of Pharmacy, Ajou University, Suwon 16499, Korea; [3]Targeted Medicine Research Center, Korea Research Institute of Bioscience and Biotechnology, Cheongwon, Chungbuk 28116, and Department of Biomolecular Science, University of Science and Technology, Daejeon 34554, Korea; [4]Cancer Cell and Molecular Biology Branch, Research Institute, and Department of System Cancer Science, Graduate School of Cancer Science and Policy, National Cancer Center, Goyang 10408, Korea; [5]School of Biological Sciences, Ulsan National Institute of Science and Technology (UNIST), Ulsan 44919, Korea

Abstract

Resveratrol (3,5,4′-trihydroxy-*trans*-stilbene) is a well-known polyphenol that is present in grapes, peanuts, pine seeds, and several other plants. Resveratrol exerts deleterious effects on various types of human cancer cells. Here, we analyzed the cell death-inducing mechanisms of resveratrol-006 (Res-006), a novel resveratrol derivative in human liver cancer cells *in vitro*. Res-006 suppressed the viability of HepG2 human hepatoma cells more effectively than resveratrol (the IC_{50} values were 67.2 and 354.8 μmol/L, respectively). Co-treatment with the ER stress regulator 4-phenylbutyrate (0.5 mmol/L) or the ROS inhibitor *N*-acetyl-*L*-cysteine (NAC, 1 mmol/L) significantly attenuated Res-006-induced HepG2 cell death, suggesting that pro-apoptotic ER stress and/or ROS may govern the Res-006-induced HepG2 cell death. We further revealed that treatment of HepG2 cells with Res-006 (65 μmol/L) immediately elicited the dysregulation of mitochondrial dynamics and the accumulation of mitochondrial ROS. It also collapsed the mitochondrial membrane potential and further induced ER stress and cell death. These events, except for the change in mitochondrial morphology, were prevented by the exposure of the HepG2 cells to the mitochondrial ROS scavenger, Mito-TEMPO (300–1000 μmol/L). The results suggest that Res-006 may kill HepG2 cells through cell death pathways, including the ER stress initiated by mitochondrial ROS accumulation. The cell death induced by this novel resveratrol derivative involves crosstalk between the mitochondria and ER stress mechanisms.

Keywords: resveratrol; resveratrol-006; HepG2 human hepatoma cells; mitochondria; ROS; endoplasmic reticulum stress; 4-phenylbutyrate; NAC; Mito-TEMPO; apoptosis

Acta Pharmacologica Sinica (2017) 38: 1486–1500; doi: 10.1038/aps.2017.106; published online 10 Aug 2017

Introduction

Resveratrol (3,5,4′-trihydroxy-*trans*-stilbene; Res) is a nonflavonoid polyphenol present in grapes, peanuts, berries, and the constituents of several other plants[1]. It possesses a wide range of beneficial effects, including anti-cancer, anti-aging, anti-atherogenic, anti-inflammatory and anti-oxidant activities[1-3]. However, its utilization and development in products have been hampered by its poor solubility, poor chemical stability, and low bioavailability[4, 5]. Many attempts have sought to improve the bioactivity and bioavailability of Res[6, 7]. For example, trimethylated Res is up to 100-fold more cytotoxic than unamended Res in cancer cell lines due to the depletion of the intracellular pool of polyamines and altered microtubule polymerization[8].

Mitochondria are essential in cellular energy metabolism and are now recognized as being central in apoptotic cell death. Stresses, including growth-factor withdrawal, DNA

# These authors contributed equally to this work.
*To whom correspondence should be addressed.
E-mail shback@ulsan.ac.kr
Received 2017-01-17 Accepted 2017-05-19

damage, and exposure to certain chemotherapeutic agents, activate mitochondria-mediated intrinsic apoptosis pathways[9]. During intrinsic apoptosis signaling, mitochondrial outer membrane permeabilization (MOMP) leads to the release of pro-apoptotic proteins (cytochrome *c*, Smac/DIABLO, Omi/HtrA2, AIF and endonuclease G) contained in the intermembrane space[9]. These pro-apoptotic proteins trigger the execution of cell death by promoting the caspase activation cascade or by acting as caspase-independent death effectors[9]. Several recent reports suggested that Res and its derivatives trigger apoptosis through the intrinsic mitochondrial-dependent pathway, which is associated with mitochondrial dysfunctions, such as mitochondrial membrane potential (MMP) collapse and reactive oxygen species (ROS) production[10-12].

The endoplasmic reticulum (ER) is a principal cellular compartment for the biosynthesis, folding and modification of membrane and secretory proteins, production of lipids and sterols, and calcium storage and gated release in eukaryotic cells. The pathological, environmental, or physiological stimuli that interfere with ER functions cause ER stress. To cope with the ER stress conditions, the ER activates a set of signal transduction pathways, collectively termed the unfolded protein response (UPR), to assist with protein folding and secretion and to facilitate the degradation of misfolded proteins in the ER lumen[13]. In mammals, the UPR is mediated by three basic signal transducers: inositol-requiring 1α (IRE1α), PERK (double-strand RNA-activated protein kinase-like ER kinase), and ATF6α (activating transcription factor 6α)[13, 14]. During ER stress, the cytoplasmic nuclease domain of activated IRE1α processes the mRNA encoding the XBP-1 (X-box-binding protein 1) transcription factor to generate mature *Xbp1* mRNA (*Xbp1s*)[15]. The activated PERK phosphorylates the α subunit of eukaryotic translation initiation factor 2 (eIF2α) at Ser51 to attenuate global translation[16] and increase the translation of mRNAs, such as those encoding the ATF4 transcription factor[17]. Upon activation, ATF6α translocates from the ER to the Golgi complex, where it is cleaved by the S1P and S2P proteases to release a cytosolic fragment (ATF6αΔC) that migrates to the nucleus to activate transcription[18, 19]. For ER stress adaptation, XBP1s and ATF6αΔC by themselves or together induce many UPR genes to enhance ER protein folding, trafficking, secretion, and ER-associated protein degradation (ERAD)[20, 21]. ATF4 induces the expression of several genes involved in amino acid biosynthesis and transport, anti-oxidative stress, and ER protein folding and secretion[22]. However, if the ER stress is too strong and persistent to re-establish ER homeostasis, the ER preferentially elicits several cell-death signaling pathways, including three UPR pathway-mediated apoptosis pathways, over time[23, 24]. Under chronic ER stress, IRE1α recruits the tumor necrosis factor receptor-associated factor 2 (TRAF2) and apoptosis signal-regulating kinase 1 (ASK1) and then causes the activation of c-Jun N-terminal kinase (JNK), which is implicated in apoptosis[25, 26]. In addition, prolonged IRE1α-mediated activation of the regulated IRE1-dependent decay (RIDD) pathway may promote apoptosis by degrading mRNAs encoding essential ER-translocating proteins[27] and microRNAs repressing the translation of pro-apoptotic *caspase-2* mRNA[28]. Although the PERK-eIF2α phosphorylation-ATF4 and ATF6α pathways conduct important adaptive mechanisms to relieve the ER stress, ATF4 and ATF6αΔC converge on the promoter of the gene encoding C/EBP homologous protein (CHOP)[21, 29], an important pro-apoptotic transcription factor of ER stress-mediated cell death[23], which controls the expression of the pro-apoptotic (*Bim*)[30] and anti-apoptotic (*Bcl-2*) genes[31]. Furthermore, CHOP expression increases the expression of several pro-apoptotic genes, such as ER oxidoreductase 1-α (ERO1α), growth arrest and DNA damage 34 (GADD34), tribbles-related protein3 (Trb3) and death receptor 5 (Dr5)[23].

A growing body of data indicates that Res and Res derivatives can induce pro-apoptotic ER stress in cancer cells by disrupting the N-linked glycosylation of proteins or by increasing intracellular calcium levels[32-34]. Here, we sought to detect the cell death effects of a new Res derivative in a human liver cancer cell line and to determine the underlying mechanism of its activity, which involves apoptosis associated with mitochondrial dysfunctions and ER stress.

Materials and methods

Reagents and antibodies

Resveratrol (Res), N-acetyl-*L*-cysteine (NAC), 4-phenylbutyric acid (4-PBA), BAPTA-AM, TEMPOL, Mito-TEMPO, and Hoechst 33258 were purchased from Sigma-Aldrich (St Louis, MO, USA). Tunicamycin and thapsigargin were purchased from EMD Millipore (Billerica, MA, USA). MitoTracker Red and JC-1 were purchased from Molecular Probes (Eugene, OR, USA). Resveratrol-005 (Res-005) and resveratrol-006 (Res-006, Korea Patent #1016328390000) were synthesized by Prof Hyoungsu KIM (see Supplementary information for details). A Cell Counting Kit-8 (CCK-8) was purchased from Dojindo Molecular Technology (Rockville, MD, USA). The antibodies, including anti-BAK, anti-BAX, anti-Bcl-2, anti-Bcl-xL, anti-cleaved caspase-3, anti-CHOP, anti-IRE1α, anti-JNK, anti-p-JNK, anti-PARP, and anti-PERK, were purchased from Cell Signaling Technology (Danvers, MA, USA). Anti-β-actin and horseradish peroxidase-conjugated anti-Flag were purchased from Sigma-Aldrich (St Louis, MO, USA). In addition, the following antibodies were used: anti-eIF2α from Santa Cruz Biotechnology (Dallas, TX, USA), anti-BiP from BD Bioscience (San Jose, CA, USA), anti-KDEL from Assay Designs (Farmingdale, NY, USA), anti-p-IRE1α from Novus Biologicals (Littleton, CO, USA), anti-MTCO1 and anti-SDHA from Abcam (Cambridge, UK), and anti-p-eIF2α from Invitrogen (Carlsbad, CA, USA). The secondary peroxidase-conjugated antibodies were purchased from Thermo Fisher Scientific (Waltham, MA, USA) or Jackson ImmunoResearch (West Grove, PA, USA).

Cell culture

HepG2 human hepatocellular carcinoma cancer cells were obtained from the American Type Culture Collection (ATCC, Manassas, VA, USA). The Huh-7 cells were provided by Dr

Sung Key JANG (Department of Life Sciences, Pohang University of Science and Technology (POSTECH), Korea)[35]. Both the HepG2 and Huh-7 cells were cultured in DMEM (Gibco, Waltham, MA, USA) supplemented with 10% fetal bovine serum (ATCC) and 5% penicillin-streptomycin (Gibco). The THLE-2 cells (ATCC) originated from human primary normal liver cells and were provided by Dr Jong-heon KIM (Cancer Cell and Molecular Biology Branch, National Cancer Center, Korea). THLE-2 cells were plated on culture plates precoated with a solution containing 0.01 mg/mL fibronectin (Thermo Scientific, Waltham, MA, USA), 0.03 mg/mL bovine collagen type I (Thermo Scientific), and 0.01 mg/mL bovine serum albumin (Sigma-Aldrich) dissolved in bronchial epithelial basal medium (BEBM, Lonza, Basel, Switzerland). The THLE-2 cells were cultured in BEBM supplemented with 5 ng/mL EGF (R&D Systems, Minneapolis, MN, USA), 70 ng/mL phosphoethanolamine (Sigma-Aldrich), 10% fetal bovine serum (ATCC, Manassas, VA, USA), and BEGM SingleQuots (Lonza) with no gentamicin/amphotericin (GA) and epinephrine. The cells were grown in a 5% CO_2 incubator at 37 °C.

Cell viability assays

The cell viability assay was performed using a CCK-8 kit (Dojindo Molecular Technologies) according to the manufacturer's instructions. Briefly, the cells were plated in 96-well plates and grown overnight. The next day, the cells were treated with the indicated chemicals for 24 h, and then, the cells were treated with the CCK-8 solution for 3 h. Absorbance was measured at 450 nm using a microplate reader (Molecular Devices, Sunnyvale, CA, USA).

Transfection

HepG2 cells (1×10^5) were plated in 60-mm dishes or collagen-coated 35-mm coverglass bottom dishes and cultured overnight. The next day, the flag-tagged ATF6α-expressing plasmid (pCMV-Flag3x-ATF6α, a kind gift from Ron Prywes, Addgene plasmid #11975) or mitochondria-targeted EYFP-expressing plasmid (pEYFP-Mito, Clontech, Mountain View, CA, USA) was transfected into HepG2 cells using the Fugene6 transfection reagent (Promega, Madison, WI, USA) for 48 h. The cells were treated with the chemicals (Tm, Tg, or Res-006) for the indicated time.

Western blot analysis

Cells were lysed with NP40 lysis buffer (1% Nonidet P-40, 0.05% sodium dodecyl sulfate, 50 mmol/L Tris-Cl pH 7.5, 150 mmol/L NaCl, 0.5 mmol/L sodium vanadate, 100 mmol/L sodium fluoride, and 50 mmol/L β-glycerophosphate) supplemented with Halt protease inhibitor cocktail (Thermo Fisher Scientific, Waltham, MA, USA). The homogenates were centrifuged at 12 000×*g* for 15 min at 4 °C, and the supernatants were collected. The protein concentration was determined using a BCA protein assay kit (Bio-Rad, Hercules, CA, USA). Protein samples were resolved by sodium dodecyl sulfate-polyacrylamide gel electrophoresis and transferred to polyvinylidene difluoride or nitrocellulose membranes (GE Healthcare Life Sciences, Marlborough, MA, USA). The membranes were blocked for 3 h at room temperature with 5% skim milk in Tris-buffered saline Tween buffer (0.1% Tween 20, 20 mmol/L Tris-HCl, pH 7.5, and 150 mmol/L NaCl). The membranes were then incubated with the indicated primary antibodies overnight at 4 °C and then with the horseradish peroxidase-conjugated secondary antibody. Membrane-bound antibodies were detected by enhanced chemiluminescence (ECL) (Thermo Scientific).

Flow cytometry analysis of apoptosis or the cellular ROS level

HepG2 cells (2×10^5) were plated in 6-well plates and cultured overnight. The cells were treated with the indicated chemicals. After treatment, the cells were harvested and then washed twice with cold-phosphate buffered saline (PBS). Next, the cells were double-stained with annexin V and 7-aminoactinomycin D (7AAD) (BD Pharmingen, Franklin Lakes, NJ, USA) in binding buffer for 15 min. Finally, the cells were analyzed by flow cytometry using a FACSCanto II apparatus (BD Biosciences, Franklin Lakes, NJ, USA). FlowJo software (Ashland, OR, USA) was used for the analysis. HepG2 cells (2×10^5) were plated in 6-well plates and cultured overnight. The next day, the cells were treated with the indicated chemicals. After treatment, the cells were stained with dihydroethidium (15 μmol/L, Sigma-Aldrich) in culture medium for 30 min. The cells were harvested and analyzed by flow cytometry as described above.

Immunofluorescence

HepG2 cells (2×10^5) were plated in 6-well plates coated with collagen 0.01% in PBS and cultured overnight. The next day, the cells were treated with the indicated chemicals, fixed with 4% paraformaldehyde in PBS for 15 min, and permeabilized with 0.2% Triton X-100 in PBS for 2 min. The cells were blocked with 1% bovine serum albumin in PBS for 30 min and incubated with the indicated primary antibody overnight at 4 °C. The cells were further incubated with a fluorescein isothiocyanate-conjugated secondary antibodies at room temperature for 1 h. The nuclei were stained with Hoechst 33258 (Sigma-Aldrich). Finally, the cells were observed by confocal laser microscopy using an FV1200-OSR microscope (Olympus, Tokyo, Japan).

Mitochondrial membrane potential (MMP) analysis

THLE-2 and HepG2 cells (2×10^5) were plated in collagen-coated 35 mm coverglass bottom dishes (SPL, Pocheon-si, Gyeonggi-do, Korea) and cultured overnight. The next day, the cells were treated with the indicated chemicals. After treatment, the cells were stained with MitoTracker Red (200 nmol/L) or JC-1 (2.5 μmol/L) and Hoechst 33258 (4 μg/mL) in culture medium for 1 h. Fluorescence images of living cells were obtained using an FV1200-OSR confocal laser microscope.

Time-lapse confocal microscopy

Mitochondria-targeted EYFP-expressing HepG2 cells were

treated with mock or Res-006 for 20 min, and then the mitochondria were imaged for 4 min and 30 s using an FV1200-OSR confocal laser microscope (Olympus). Frames were taken every 30 s. The microscopic field was 63.4 μm×63.4 μm.

Semi-quantitative PCR and qRT-PCR

Total RNA was prepared from the HepG2 cells treated with the indicated chemicals using an RNeasy Plus Mini Kit (Qiagen, Venlo, Netherlands). The cDNA was prepared with a High Capacity cDNA RT Kit (Ambion, Life Technologies, Waltham, MA, USA) for semi-quantitative PCR using standard methods or for qRT-PCR normalized to the levels of β-actin as previously described[36]. The primers for the semi-quantitative PCR analysis were as follows: forward primer for *Xbp1* mRNA splicing analysis, 5′-CCGCAGCAGGTGCAGG-3′ and reverse primer 5′-GGGGCTTGGTATATATGTGG-3′; forward primer for *Gapdh* mRNA, 5′-ACATCAAGAAGGTGGTGAAG-3′ and reverse primer 5′-CTGTTGCTGTAGCCAAATTC-3′. The primers for the qRT-PCR analysis are as follows: *β-actin* forward primer 5′-TCCCCCAACTTGAGATGTATGAAG-3′ and *β-actin* reverse primer 5′-AACTGGTCTCAAGTCAGTGTACAGG-3′; *Xbp1s* forward primer 5′-CCGCAGCAGGTGCAGG-3′ and *Xbp1s* reverse primer 5′-GAGTCAATACCGCCAGAATCCA-3′; *Xbp1t* forward primer 5′-GCAAGCGACAGCGCCT-3′ and *Xbp1t* reverse primer 5′-TTTTCAGTTTCCTCCTCAGCG-3′; *ERdj4* forward primer 5′-GGAAGGAGGAGCGCTAGGTC-3′ and *ERdj4* reverse primer 5′-ATCCTGCACCCTCCGACTAC-3′; *Chop* forward primer 5′-ATGGCAGCTGAGTCATTGCCTTTC-3′ and *Chop* reverse primer 5′-AGAAGCAGGGTCAAGAGTGGTGAA-3′; and *Grp78* (*BiP*) forward primer 5′-GCCTGTATTTCTAGACCTGCC-3′ and *Grp78* (*BiP*) reverse primer 5′-TTCATCTTGCCAGCCAGTTG-3′.

Statistical analysis

All data are represented as the mean±SEM of three or four independent experiments. The data were analyzed using GraphPad Prism 5 (GraphPad Software, Inc, La Jolla, CA, USA). Unpaired 2-tailed Student's *t*-tests were performed to determine the statistical significance for paired samples. $P<0.05$ was considered significant.

Results

Res derivative 3,5-diethoxy-3′,4′-dihydroxy-*trans*-stilbene displays ER stress and/or oxidative stress-mediated cytotoxicity in HepG2 cells

To investigate the cytotoxic effect of Res and its derivatives (Figure 1A), one normal human liver cell line, THLE-2, and two human hepatoma cell lines, Huh-7 and HepG2, were treated with various concentrations of the compounds (Figure 1B-1H). The dehydrogenase-based cell viability assay revealed that the Res derivative designated Res-006 had stronger cellular toxicity than Res and Res-005 in all cell lines used (Figure 1B, 1D, 1F, and 1G). The IC_{50} value (67.2 μmol/L) of Res-006 in HepG2 cells was approximately 2-fold lower than that (139.2 μmol/L) in THLE-2 cells (Figure 1C, 1E, and 1G). The cytotoxic effect of 65 μmol/L Res-006 against HepG2 cells was higher than that against THLE-2 and Huh-7 cells (Figure 1H). In addition, the time-dependent expression of apoptotic marker proteins (cleaved caspase-3 and PARP) in lysates of Res-006-treated HepG2 cells was higher compared with that of Res-006-treated THLE-2 and Huh-7 cells (Figure 1I). Therefore, subsequent experiments were focused on the cytotoxic effects of Res-6 against HepG2 cells.

To investigate whether Res-006 can induce apoptosis in HepG2 cells, we examined the apoptotic effect of Res-006 by flow cytometry and Western blot analyses. In the mock-treated group, <6.0% of cells underwent apoptosis (Q2+Q4 in Figure 2A). In contrast, in cells treated with 65 μmol/L Res-006, 26.1% of cells underwent apoptosis (Figure 2A). Moreover, both caspase-3 and PARP were significantly cleaved and activated by Res-006 (Figure 2B). The results indicated that Res-006 can significantly induce apoptosis in HepG2 cells.

Several recent reports suggested that Res and its derivatives can elicit ER stress-mediated cell death[32] by increasing the level of cellular calcium by inhibiting sarco/endoplasmic reticulum Ca^{2+} ATPase (SERCA)[34] or disrupting the *N*-linked glycosylation of proteins[33]. In addition, oxidative stress induced by the drugs may be responsible for cell death[12, 37]. To verify whether ER stress and/or oxidative stress are associated with Res-006-mediated HepG2 cell death, the ER stress regulator 4-phenylbutyrate (PBA) and/or the ROS inhibitor N-acetyl-*L*-cysteine (NAC) were applied along with Res-006. Inhibition of either ER stress or ROS antagonized the cell death activity of Res-006 toward HepG2 cells (Figure 2C). Moreover, compared with the treatment with drug alone, co-treatment with 4-PBA and NAC further increased cell viability (Figure 2C), indicating that pro-apoptotic ER stress and/or ROS may govern the cell death induced by Res-006 in HepG2 cells. However, treatment with the Ca^{2+} chelator BAPTA/AM did not restore the viability of Res-006-treated HepG2 cells (Figure 2D), suggesting that an increase in intracellular Ca^{2+} levels may not relate with Res-006-mediated cell death. Next, to determine the effect of Res-006 on the N-linked glycosylation of the proteins, we monitored the N-linked glycosylation of ATF6α, an N-linked glycosylated ER membrane protein[18] in HepG2 cells. Tunicamycin (Tm), an established inhibitor of N-linked glycosylation[38], was used to generate a positive control. The 3xFlag-tagged human ATF6α proteins were transiently overexpressed in HepG2 cells. The deglycosylation-induced mobility change of 3xFlag-ATF6α was examined by Western blot analysis with tunicamycin, the SERCA inhibitor thapsigargin (Tg), or Res-006-treated HepG2 cells. As expected, the 3xFlag-ATF6α in the Tm-treated cell lysates migrated faster compared with the mock or Tg-treated cell lysates (Figure 2E), indicating that the protein was deglycosylated by tunicamycin treatment. However, there were no fast migrating bands observed in Res-006-treated lysates until 24 h (Figure 2E), suggesting that the Res-006 may not elicit ER stress through the disruption of the N-linked glycosylation of the proteins. Taken together, these results suggest that Res-006 induces ER stress- and/or ROS-mediated cell death, which is not associated with acute cal-

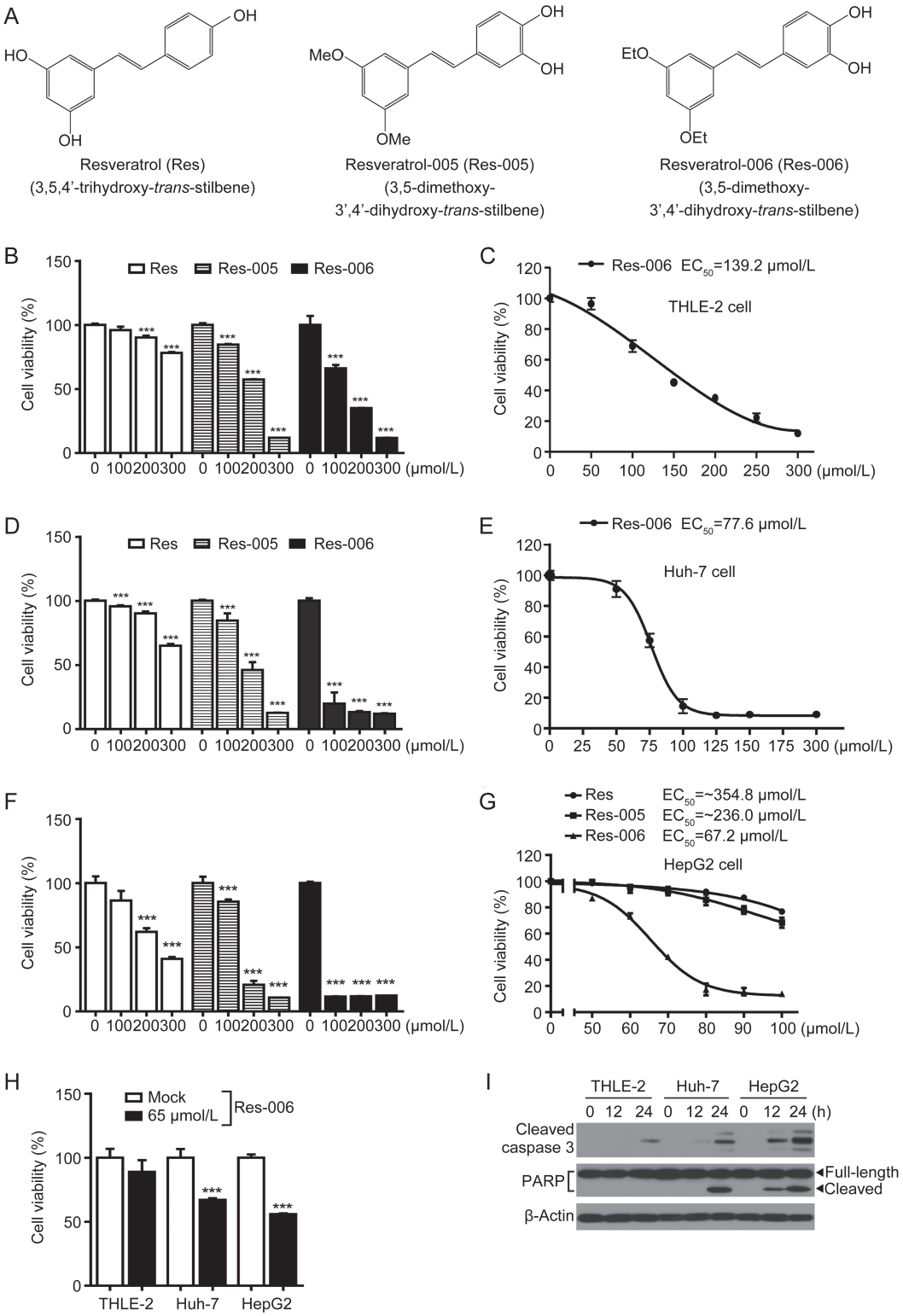

Figure 1. Res-006 exhibits a higher cytotoxic activity than Res and Res-005 in hepatocellular carcinoma cells. (A) Chemical structures of Res and the two derivatives. (B), (D), and (F) THLE-2, Huh-7, and HepG2 cells were treated with Res, Res-005, or Res-006 (0–300 μmol/L) for 24 h, and cell viability was analyzed by the CCK-8 assay. The data are expressed as the mean±SEM of three independent experiments, $^{***}P<0.001$; 0 μmol/L *vs* each concentration. (C), (E), and (G) Dose response curves and EC_{50} values of Res-006 for THLE-2, Huh-7, and HepG2 cells. The data are expressed as the mean±SEM of three independent experiments. (H) THLE-2, Huh-7, and HepG2 cells were treated with Res-006 (65 μmol/L) for 24 h, and cell viability was analyzed by the CCK-8 assay. The data are expressed as the mean±SEM of three independent experiments, $^{***}P<0.001$; Mock-treated cells *vs* Res-006-treated cells. (I) THLE-2, Huh-7, and HepG2 cells were treated with Res-006 (65 μmol/L) for the indicated times, and total cellular extracts were prepared and subjected to Western blot analysis.

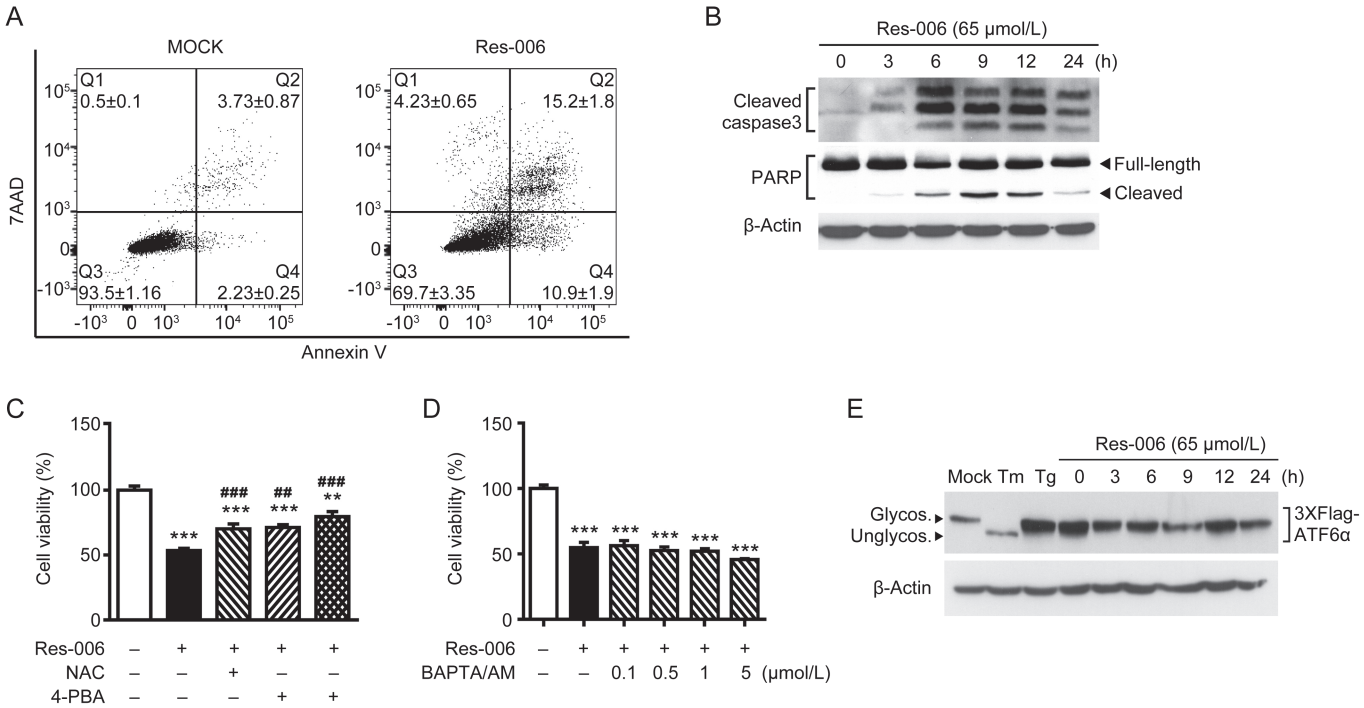

Figure 2. Res-006 induces cell death associated with ER stress and/or ROS in HepG2 cells. (A) Flow cytometry analysis of cell death after Res-006 (65 μmol/L) treatment for 24 h. Representative images are shown (n=3 per group). (B) HepG2 cells were treated with Res-006 (65 μmol/L), and total cellular extracts were prepared and subjected to Western blot analysis. (C) HepG2 cells were treated with Res-006 (65 μmol/L), Res-006 (65 μmol/L), and NAC (1 mmol/L), or with Res-006 (65 μmol/L) and 4-PBA (0.5 mmol/L) for 24 h, and the cell viability was analyzed by the CCK-8 assay. The data are expressed as the mean±SEM of three independent experiments, $^{**}P$<0.01 and $^{***}P$<0.001; untreated group *vs* each treated group, $^{\#\#}P$<0.01 and $^{\#\#\#}P$<0.001; Res-006-treated group *vs* each treated group. (D) HepG2 cells were cotreated with Res-006 (65 μmol/L) and BAPTA/AM (0–5 μmol/L) for 24 h, and cell viability was analyzed using the CCK-8 assay. The data are expressed as the mean±SEM of three independent experiments, $^{***}P$<0.001; untreated group *vs* each treated group. (E) HepG2 cells were transfected with pCMV-Flag3x-ATF6α for 48 h and then treated with Res-006 (65 μmol/L) for the indicated times or were mock treated, with Tm (10 μg/mL) and Tg (1 μmol/L) for 12 h, and total cellular extracts were prepared and subjected to Western blot analysis.

cium mobilization or N-linked glycosylation inhibition.

Res-006 dysregulates mitochondrial dynamics and disrupts MMP in HepG2 cells

It is possible that mitochondrial dysfunction can induce ER stress[37, 39] and vice versa[24, 40, 41]. To explore this, we first used mitochondria-targeted enhanced yellow fluorescent protein (Mito-EYFP) to monitor the morphological changes of mitochondria during Res-006 treatment in HepG2 cells (Figure 3A). Following the addition of Res-006, the mitochondrial morphology changed from interconnected filaments to large spheres within 60 min, whereas the morphology was barely changed in the mock-treated cells (Figure 3A). Because mitochondrial morphology is determined by a dynamic equilibrium between organelle fusion and fission, we imaged mitochondria for 4.5 min in mock-treated and Res-006-treated cells (Figure 3B and Supplementary Movie S1 and S2). In the mock-treated cells, the mitochondria were highly mobile, and several fusion and fission events were observed during the recordings (Supplementary Movie S1). However, in the Res-006-treated cells, many mitochondria had already become ovoid or spherical, possibly due to fusion before the time-lapse experiments. Later on, the fusion or fission events were rarely observed. One fusion event was observed, which generated a large spherical mitochondrion (arrows and ovals in Figure 3B and Supplementary Movie S2). In addition to reduced fusion and fission, the time-lapse videos revealed striking defects in the mobility of the mitochondria in Res-006-treated HepG2 cells. These results suggest that Res-006 alters mitochondrial dynamics, which can lead to a mitochondrial morphology change.

Next, we tested whether Res-006 treatment could disrupt MMP, which is an important parameter of mitochondrial function. MitoTracker Red, a lipophilic cationic dye that is sensitive to the MMP, was used to stain Res-006-treated HepG2 cells. The number of stained mitochondria and their fluorescence intensities were gradually reduced in Res-006-treated cells until 24 h; however, they were not changed in mock-treated cells (Figure 3C and 3E) and Res-006-treated THLE-2 cells (Supplementary Figure S1). However, the levels of the mitochondrial DNA-encoded protein MTCO1 and a nuclear-encoded protein SDHA remained unchanged in Res-006-treated HepG2 cells until 24 h (Figure 3D). In addition, immunofluorescence analysis of MTCO1 showed that the fluorescence intensity of mitochondria labeled with the anti-

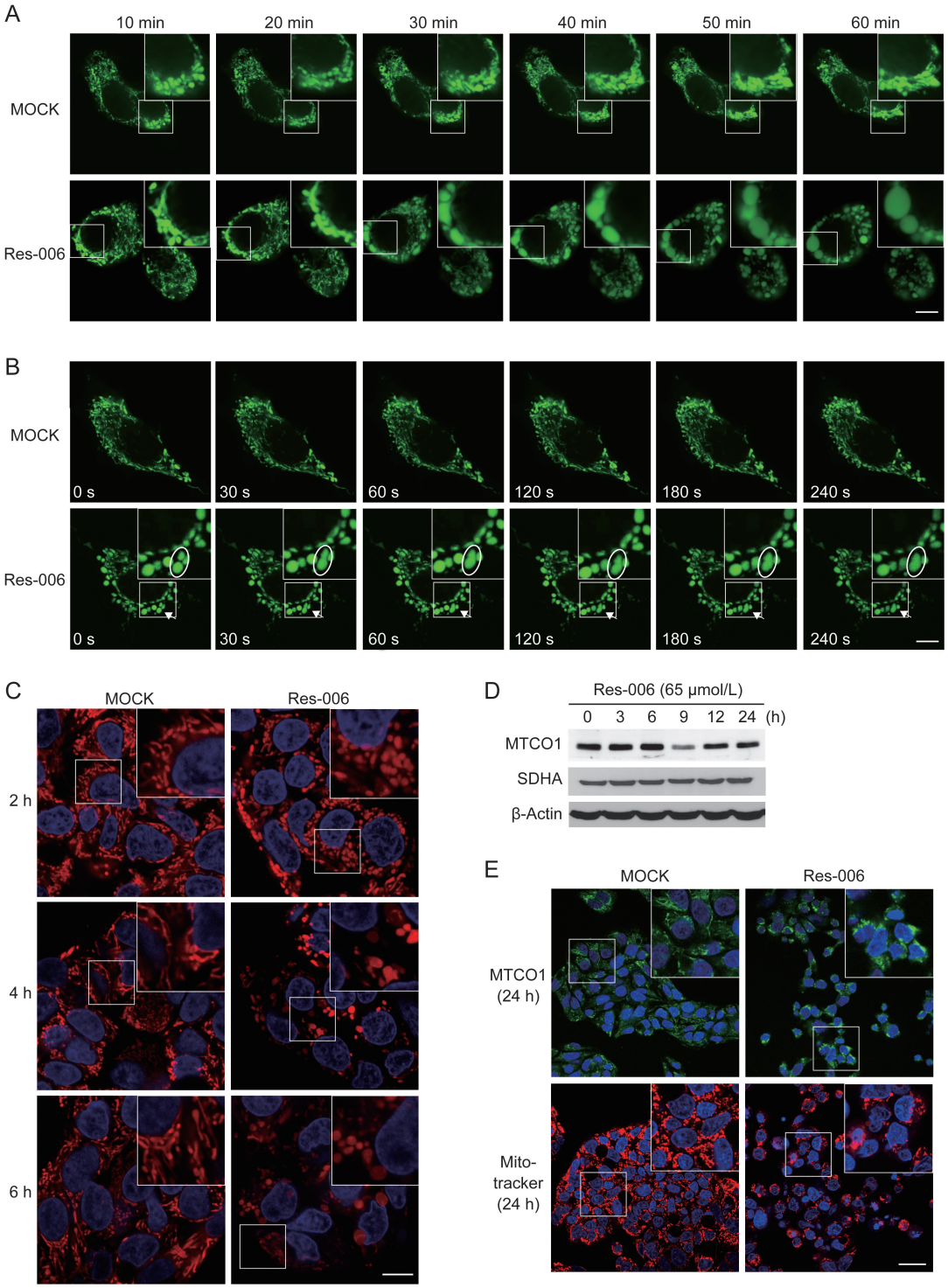

Figure 3. Res-006 dysregulates mitochondrial dynamics and disrupts MMP in HepG2 cells. (A and B) HepG2 cells transfected with a Mito-EYFP-expressing plasmid (pEYFP-Mito) were treated with Res-006 (65 μmol/L), and the mitochondrial dynamics were analyzed by confocal fluorescence microscopy at the designated times. The scale bar denotes 10 μm. Inset shows a magnified view of the area outlined in the white lined box. The ovals in (B) outline mitochondria that are in the process of fusing. (C) HepG2 cells were stained with Hoechst 33258 (blue fluorescence, 2.5 μg/mL) and MitoTracker Red (200 nmol/L) after treatment with Res-006 (65 μmol/L) and were analyzed by confocal fluorescence microscopy at the indicated times. The scale bar denotes 10 μm. Inset shows a magnified view of the area outlined in the white lined box. (D) HepG2 cells were treated with Res-006 (65 μmol/L). Total cellular extracts were prepared and analyzed using Western blotting for MTCO1 (mitochondrially encoded cytochrome c oxidase I), SDHA (succinate dehydrogenase complex, subunit A), and β-actin. (E) HepG2 cells were stained with Hoechst 33258 (blue fluorescence) and anti-MTCO1 antibodies (green fluorescence) or Hoechst 33258 and MitoTracker Red after Res-006 treatment for 24 h and analyzed by confocal fluorescence microscopy. The scale bar denotes 30 μm. Inset shows a magnified view of the area outlined in the white lined box.

MTCO1 antibody did not decrease in Res-006-treated cells for 24 h compared with the mock-treated cells; whereas the fluorescence intensity of MMP-dependent MitoTracker Red was significantly decreased by the drug treatment (Figure 3E). The observations suggested that Res-006 treatment disrupts mitochondrial function but does not cause the removal of malfunctioning mitochondria from the cells.

Res-006-induced cell death is prevented by superoxide scavenger

Mitochondria are an important source of ROS within most mammalian cells[42, 43]. In addition, cellular redox homeostasis is interconnected with MMP[42, 44, 45]. The level of accumulated ROS was measured by flow cytometry following staining of the cells with the superoxide indicator dihydroethidium (DHE). The ROS levels in cells treated for 2 h with Res-006 was significantly higher (approximately 2.3 fold) than in the mock-treated cells (Figure 4A). From these results, we hypothesized that in Res-006 treated cells, the ROS accumulation leads to mitochondrial dysfunction (Figure 3A-3E) and cell death (Figure 2B), which can be ameliorated by its modulation. To verify this hypothesis, HepG2 cells were co-treated with the superoxide dismutase mimetic TEMPOL (Tem) and Res-006. The TEMPOL dose-dependently increased the viability of Res-006-treated cell populations up to approximately 80% (Figure 4B, 4D, and 4E). Given that Res-006 led to mitochondrial dysfunctions (Figure 3A-3C and 3E) associated with mitochondrial ROS generation, we next used a mitochondria-targeted TEMPOL (Mito-TEMPO, Mito) to specifically reduce the mitochondrial ROS levels. Intriguingly, the Mito-TEMPO treatments completely prevented cell death induced by Res-006 at concentrations over 300 μmol/L (Figures 4C-4E). The flow cytometry of cells stained with annexin V and 7AAD clearly showed that the Mito-TEMPO treatment nearly abrogated Res-006-induced cell death (Figure 4F). In addition, the Mito-TEMPO treatment markedly inhibited caspase-3 activation and PARP cleavage induced by Res-006, although TEMPOL also showed significant inhibitory effects against the events (Figure 4G). Taken together, these data indicate that Res-006 induces cell death, which can be prevented by the removal of mitochondrial ROS.

Mitochondria-targeted superoxide scavenger prevents Res-006-mediated MMP disruption

To explore the efficiency of the inhibition of ROS accumulation by two superoxide scavengers in Res-006-treated HepG2 cells, flow cytometry was used to examine dihydroethidium (DHE)-stained cells. Both superoxide scavengers significantly inhibited ROS accumulation induced by Res-006 treatment. Notably, the ROS levels in the Mito-TEMPO treated cells were as low as those in the mock-treated cells (Figure 5A). Next, to verify whether the increased viability due to ROS scavenging could be correlated with the recovery of MMP in Res-006-treated HepG2 cells, we used JC-1, a cationic MMP probe that accumulates in energized mitochondria. The cells that were exposed to Res-006 for 2 h displayed greatly reduced red J-aggregate fluorescence and significantly increased cytoplasmic green monomer fluorescence compared with the mock-treated cells (Figure 5B), indicating that Res-006 treatment causes the rapid collapse of MMP, which may have preceded apoptotic cell death (Figure 2B). However, both superoxide scavengers significantly restored red J-aggregate fluorescence, suggesting that ROS scavenging can prevent the MMP loss in Res-006-treated HepG2 cells (Figure 5B). In addition, the TEMPOL and Mito-TEMPO treatments greatly restored both the number and fluorescence intensities of the MitoTracker Red-stained mitochondria in Res-006-treated cells (Figure 5C); however, they did not prevent Res-006-mediated mitochondrial fragmentation and swelling, indicating that the mitochondrial morphological changes may not be related with the Res-006-mediated ROS accumulation and cell death.

Res-006 induces ER stress responses

Treatment with 4-phenylbutyric acid, an ER stress inhibitor, ameliorated Res-006-mediated cellular toxicity (Figure 2C). Thus, we investigated whether Res-006 could operate as an ER stress inducer. ROS-006 treatment induced the quick activation of all three UPR sensors (IRE1α, PERK, and ATF6α) in HepG2 cells[13, 14] (Figure 6A-6D). First, IRE1α phosphorylation[46] and its mediated downstream events, including increases in JNK phosphorylation[25], *Xbp1* mRNA splicing[47], and XBP1s-dependent *Erdj4* mRNA expression[48], occurred in Res-006-treated cells (Figure 6A and 6D). Second, Res-006 treatment induced the activation of the PERK/eIF2α-dependent pathway, including marked and persistent PERK phosphorylation, eIF2α phosphorylation at 3 h (Figure 6B), and increases in *Chop* transcripts (Figure 6D)[29, 49] and CHOP proteins (Figure 6B)[50]. Third, the activation of the last UPR sensor ATF6α was determined by the observation of the S1P and S2P protease-mediated cleavage fragment (3XFlag-ATF6αΔC) generated[19] from Flag-tagged ATF6α protein exogenously expressed in Res-006-treated HepG2 cells (Figure 6C). As expected, the level of the cleavage product (3XFlag-ATF6αΔC) was increased in the HepG2 cells treated with the ER stress inducer, dithiothreitol (DTT) (Figure 6C)[18, 19]. Similarly, the Flag-tagged cleavage products increased over time in the Res-006-treated HepG2 cells. Furthermore, consistent with the ATF6α activation, the Res-006 treatment significantly increased the expression of an ATF6α downstream target gene *Grp78* (Figure 6C and 6D)[20, 21]. Taken together, these results clearly suggest that Res-006 is a strong ER stress inducer that can activate all three UPR pathways in HepG2 cells.

Res-006 induces mitochondrial ROS-mediated ER stress

Since the removal of mitochondrial ROS prevented Res-006-mediated cell death, we questioned whether mitochondrial ROS scavenging can reduce ER stress responses in Res-006-treated HepG2 cells. Mitochondria-targeted Mito-TEMPO treatment significantly prevented IRE1α and JNK phosphorylation (Figure 7A). It strongly inhibited IRE1α-mediated *Xbp1* mRNA splicing (Figure 7B) and subsequent expression of *Erdj4*, an XBP1s target gene (Figure 7C) in Res-006 treated cells. In addition, the Mito-TEMPO treatment robustly inhib-

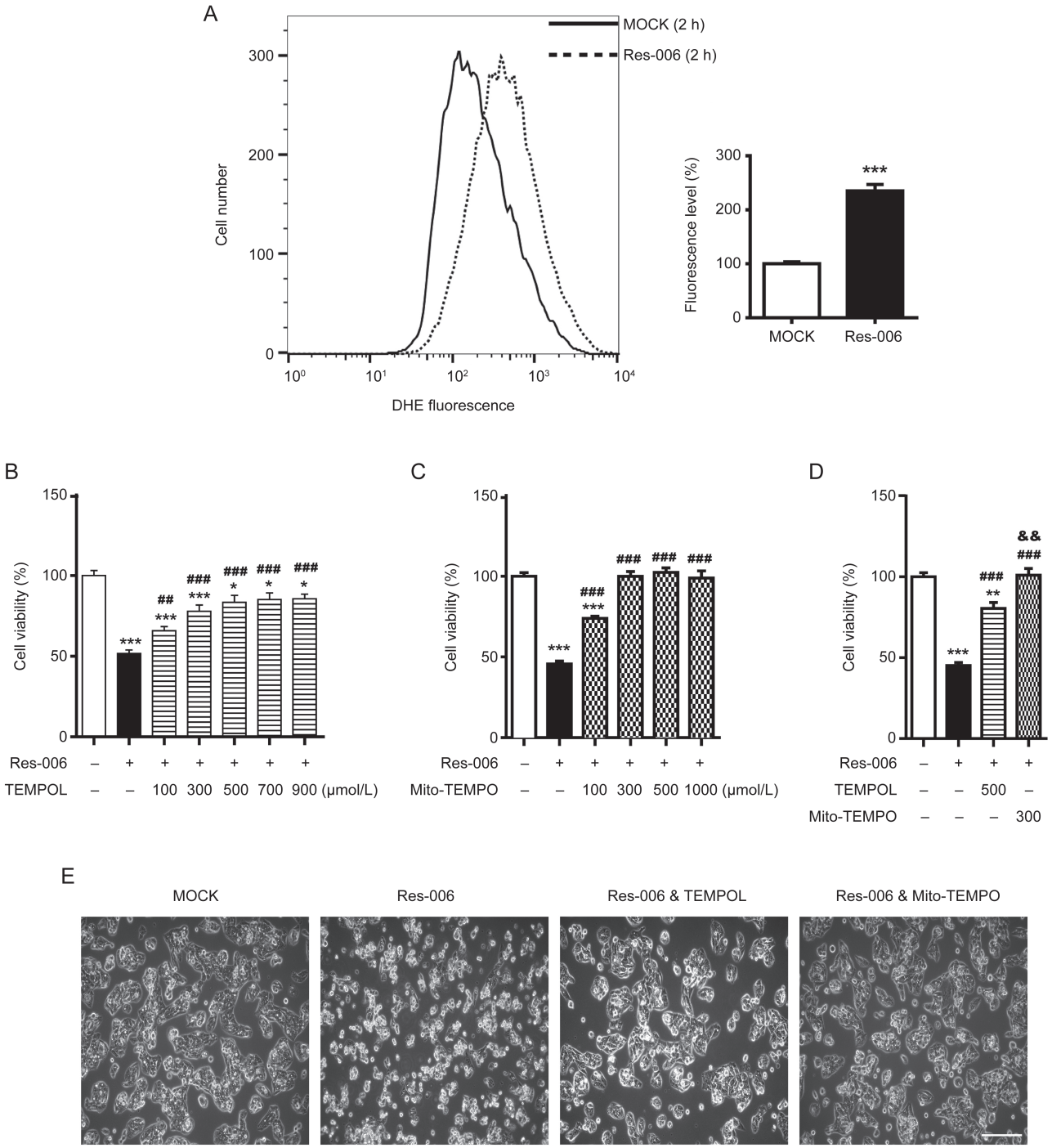

Figure 4A–4E. Res-006-induced cell death is prevented by mitochondria-targeted superoxide scavenger. (A) Flow cytometry analysis of the accumulated superoxide levels using DHE (15 μmol/L) dye in Res-006 (65 μmol/L)-treated cells. A representative image from three independent experiments is shown in the left panel. The graph shows the relative fluorescence levels of three independent samples per group. The data are expressed as the mean±SEM (*n*=3 mice per treatment). (B–D) HepG2 cells were treated for 24 h with Res-006 (65 μmol/L) only or Res-006 (65 μmol/L) and TEMPOL (100–900 μmol/L) in (B), Res-006 (65 μmol/L) only or Res-006 (65 μmol/L) and Mito-TEMPO (100–1000 μmol/L) in (C), or Res-006 (65 μmol/L) only, Res-006 (65 μmol/L) and TEMPOL (500 μmol/L), or Res-006 and Mito-TEMPO (300 μmol/L) in (D). Cell viability was analyzed using the CCK-8 assay. The data are expressed as the mean±SEM of three independent experiments, $^{*}P<0.05$ and $^{***}P<0.001$; untreated group *vs* each treated group, $^{\#\#}P<0.01$ and $^{\#\#\#}P<0.001$; Res-006-treated group *vs* each treated group, $^{\&\&}P<0.01$; Res-006- and TEMPOL-treated group *vs* Res-006- and Mito-TEMPO-treated group. (E) HepG2 cells were treated with the indicated chemicals for 24 h, and cell viability was examined using confocal microscopy. The scale bar denotes 200 μm.

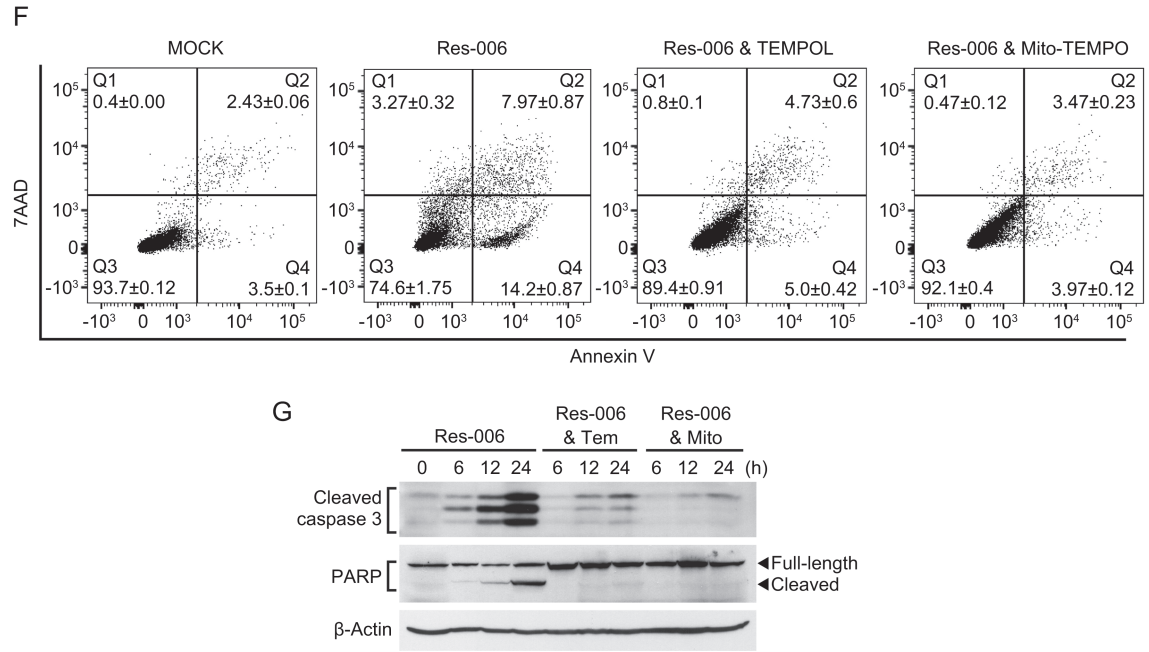

Figure 4F, 4G. Res-006-induced cell death is prevented by mitochondria-targeted superoxide scavenger. (F) Flow cytometry analysis of cell death after treatment with Res-006 (65 μmol/L) only, Res-006 (65 μmol/L) and TEMPOL (Tem, 500 μmol/L), or Res-006 (65 μmol/L) and Mito-TEMPO (Mito, 300 μmol/L) treatments for 24 h. (G) HepG2 cells were treated with the indicated chemicals, and the total cellular extracts were prepared and subjected to Western blot analysis.

ited PERK phosphorylation (Figure 7B) and strongly suppressed pro-apoptotic CHOP expression (Figure 7A and 7C). Lastly, it significantly reduced the expression of *Grp78,* an ATF6α downstream target gene (Figure 7C), suggesting that ATF6α activation was blocked by ROS scavenger treatment in Res-006-treated HepG2 cells. Although non-mitochondria-targeted TEMPOL could substantially suppress ER stress responses induced by Res-006 treatment, it was not as strong as Mito-TEMPO (Figure 7A-7C). Collectively, these results strongly support the view that mitochondrial ROS that accumulate during Res-006 treatment induces ER stress responses that can induce cell death.

Discussion

Currently, the chemical derivatization of Res produced two novel cytotoxic drugs with improved cell death activity compared with Res. Res-006 produced mitochondrial dysfunction and ER stress, which triggers the death of HepG2 cells. However, partial restoration of the mitochondrial dysfunctions via ROS scavengers, especially a mitochondria-targeted ROS scavenger (Mito-TEMPO) robustly prevented ER stress and cell death. We conclude that the pro-oxidant activity of Res-006 is critical in inducing ER stress and cell death.

The Res-006 treatment quickly induced ROS accumulation in advance of cell death (compare Figure 4A with Figure 2B), suggesting that ROS accumulation triggered cell death. If so, what is the source of ROS in Res-006-treated HepG2 cells? Treatment with the mitochondria-targeted ROS scavenger, Mito-TEMPO, robustly blocked ROS accumulation and restored MMP in Res-006-treated cells (Figure 5A and 5B), indicating that mitochondria are the main source of ROS. In addition, Res-006 treatment immediately caused a change in mitochondrial morphology, which led to large spherical mitochondria (Figure 3A and 3B and Supplementary Movie S1 and S2). The changes may have been caused by changes in mitochondrial fusion and/or fission and its movement, suggesting that the chemical alters mitochondrial dynamics. Mitochondrial morphology and dynamics are interlinked with cellular and mitochondrial redox homeostasis[51]. Cells deficient in mitochondrial fusion proteins (Mfn1, Mfn2, or Opa1) display a fragmented mitochondrial morphology and increased ROS levels and then die. Conversely, chemical or genetic inhibitions of mitochondrial fission proteins (Drp1 or Fis) induce mitochondrial elongation and reduce ROS production[51, 52]. Thus, mitochondrial fragmentation allows increases in ROS production. However, in our experimental conditions, treatment with the mitochondrial fission inhibitor, Mdivi-1, did not prevent Res-006-induced cell death, but rather inversely increased it (data not shown), suggesting that Res-006-mediated ROS production and cell death may not be related with increased mitochondrial fission. The time-lapse imaging experiments provided evidence that Res-006 can induce mitochondrial fusion at early time points, which rendered the mitochondria as large and spherical in HepG2 cells (Figure 3A and 3B, and Supplementary Movie S1 and S2). Therefore, the morphological changes of mitochondria may not be triggered by the inhibition of mitochondrial fusion proteins (Mfn1, Mfn2, or Opa1) in Res-006-treated HepG2 cells.

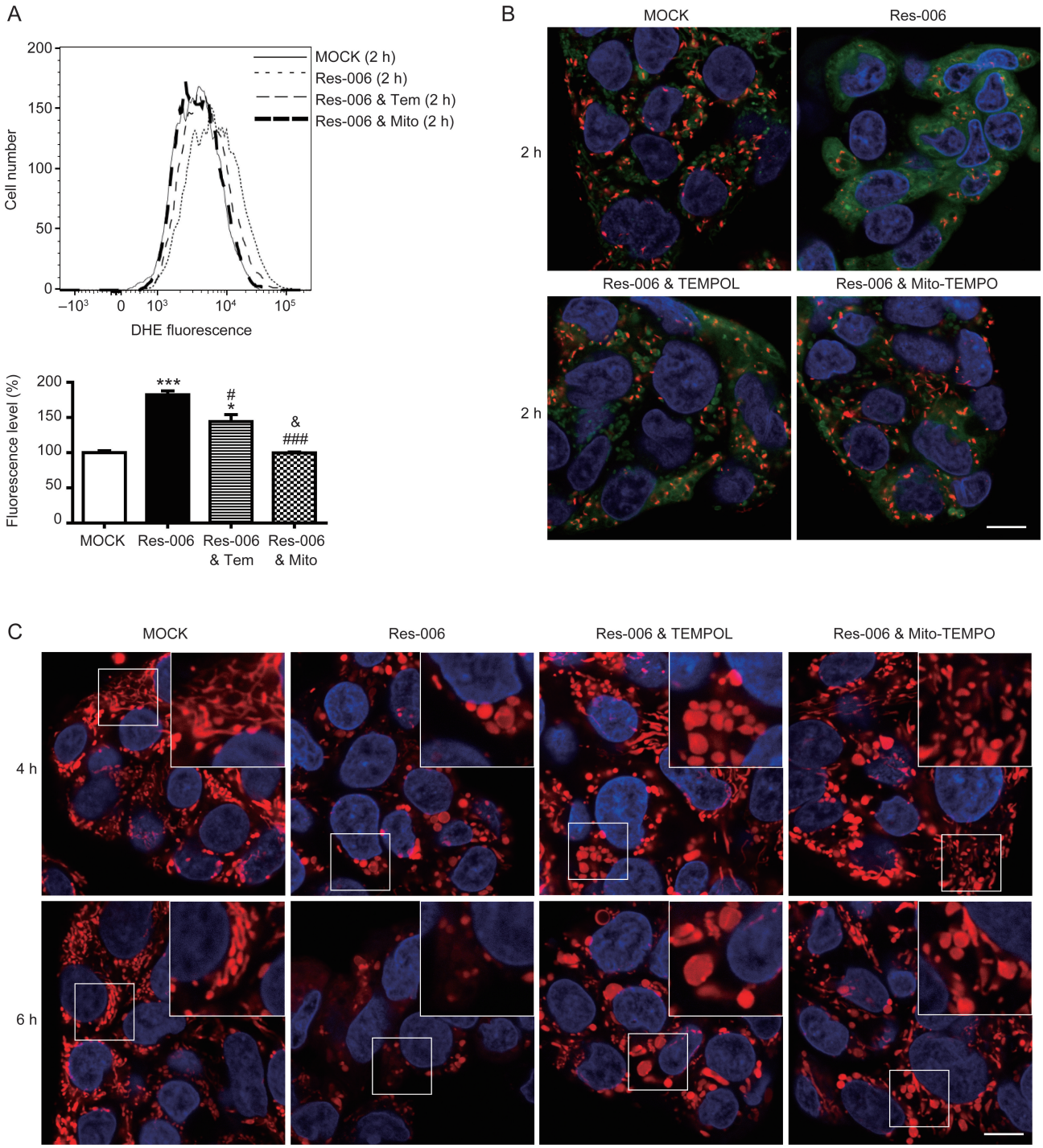

Figure 5. Mitochondria-targeted superoxide scavenger prevents Res-006-mediated disruption of MMP. (A) Flow cytometry analysis of the accumulated superoxide levels in the presence of DHE (15 μmol/L) after a 2 h treatment with Res-006 (65 μmol/L) only, Res-006 (65 μmol/L) and TEMPOL (500 μmol/L), or Res-006 (65 μmol/L) and Mito-TEMPO (300 μmol/L). A representative image from three independent experiments is shown in the upper panel. The graph shows the relative fluorescence levels of three independent samples per group. The data are expressed as the mean±SEM, $^{*}P<0.05$ and $^{***}P<0.001$; mock-treated group *vs* each treated group, $^{\#}P<0.05$ and $^{\#\#\#}P<0.001$; Res-006-treated group *vs* each treated group, $^{\&}P<0.05$; Res-006- and TEMPOL-treated group *vs* Res-006- and Mito-TEMPO-treated group. (B) HepG2 cells were stained with Hoechst 33258 and JC-1 (2.5 μmol/L) after 2-h treatments with the indicated chemicals and analyzed using confocal fluorescence microscopy. The scale bar denotes 10 μm. (C) HepG2 cells were stained with Hoechst 33258 and MitoTracker Red after treatment with Res-006 (65 μmol/L) only, Res-006 (65 μmol/L) and TEMPOL (500 μmol/L), or Res-006 (65 μmol/L) and Mito-TEMPO (500 μmol/L). Samples were analyzed by fluorescence microscopy. The scale bar denotes 10 μm. Inset shows a magnified view of the area outlined in the white lined box.

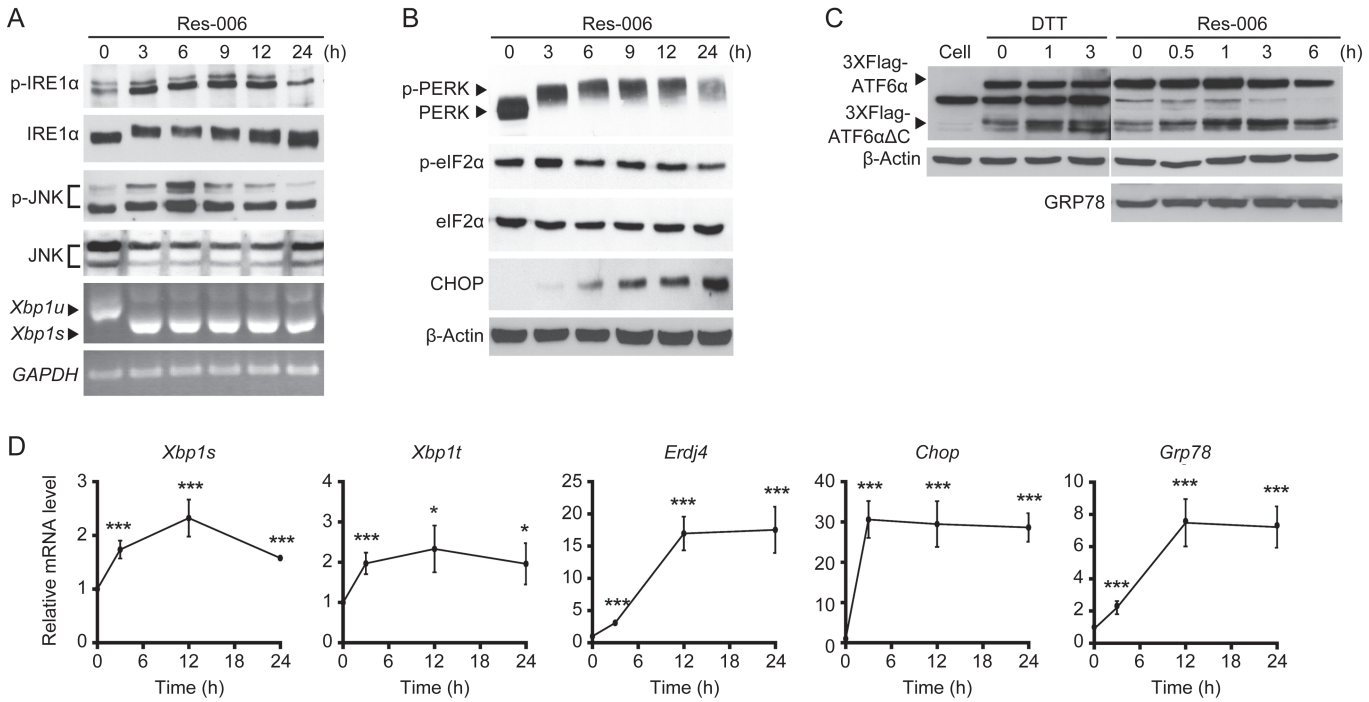

Figure 6. Res-006 is a strong ER stress inducer. (A and B) HepG2 cells were treated with Res-006 (65 μmol/L), and total cellular extracts and total RNAs were prepared and subjected to Western blot and semi-quantitative PCR analysis. (C) HepG2 cells were transfected with pCMVFlag3x-ATF6α for 48 h and then treated with DTT (5 mmol/L) or Res-006 (65 μmol/L) for the indicated times. Total cellular extracts were prepared and subjected to Western blot analysis. (D) HepG2 cells were treated with Res-006 (65 μmol/L) for the indicated times. Total RNA was prepared and subjected to quantitative real-time (qRT)-PCR analysis. The data are expressed as the mean±SEM of four independent experiments, $^{*}P<0.05$ and $^{***}P<0.001$; zero time *vs* each time.

In addition, the removal of ROS could not prevent the morphological changes of the mitochondria induced by the Res-006 treatment (Figure 5C). Thus, these data strongly suggest that ROS accumulation is not responsible for the morphological change. Inversely, it is also possible that the morphological change of mitochondria is not related with ROS accumulation and cell death in Res-006-treated HepG2 cells. The exact mechanism and role of the morphological change remain to be clarified.

Although several reports suggested that Res and its derivatives target multiple intracellular components (such as tumor suppressors p53 and Rb and apoptosis and survival regulators, Bax, Bak, AKT, Bcl-2, and Bcl-xL; see reference review[3]), including mitochondrial proteins[11, 53], which can induce mitochondrial ROS and mitochondria-mediated apoptosis pathways (Figure 7D), there is increasing evidence that Res and Res derivatives can induce ER stress and mediate cell death in several cancer cell types by disrupting the N-linked glycosylation of proteins or by increasing the level of intracellular Ca^{2+}[54]. In this study, the novel Res derivative, Res-006, also elicited ER stress. However, the ER stress inhibitor, 4-phenylbutyric acid, partially blocked Res-006-mediated ER stress (data not shown) and cell death (Figure 2C), whereas a mitochondria-targeted ROS scavenger robustly inhibited both ER stress and cell death (Figures 4C-4G and 7A-7C), indicating that the ER stress partially contributes to Res-006-mediated cell death and occurs downstream of mitochondria-ROS accumulation. Furthermore, Res-006 may not be a direct ER stress inducer inhibiting ER-mediated N-linked glycosylation or increasing intracellular calcium level because the results in Figure 2D and 2E showed that the drug-mediated cell death was not linked with the general conditions that ER stress induced.

Until now, there have been no reports that ROS accumulation caused by Res or Res derivatives can elicit ER stress, but the role of other drug-mediated mitochondrial ROS in ER stress induction has been demonstrated in a variety of cell types[39, 55]. Drug-mediated ROS generation precedes UPR induction and is efficiently blocked by ROS scavengers[55]. In terms of mechanisms, the drugs trigger mitochondrial ROS production through the regulation of gene expression or enzyme activity of mitochondrial ROS-producing proteins, such as NADPH oxidase 4 or cytochrome *c* reductase (complex III), respectively[39]. Although the precise mechanism of how mitochondrial ROS induce ER stress requires further investigation, it is proposed that oxidative protein damage and/or its mediated ER calcium release may trigger ER stress[39, 55]. However, Res-006-mediated mitochondrial ROS may not induce ER stress through the disruption of ER calcium homeostasis because treatment with the intracellular calcium chelator BAPTA/AM could not inhibit Res-006-mediated cell death (Figure 2D). This issue requires further studies.

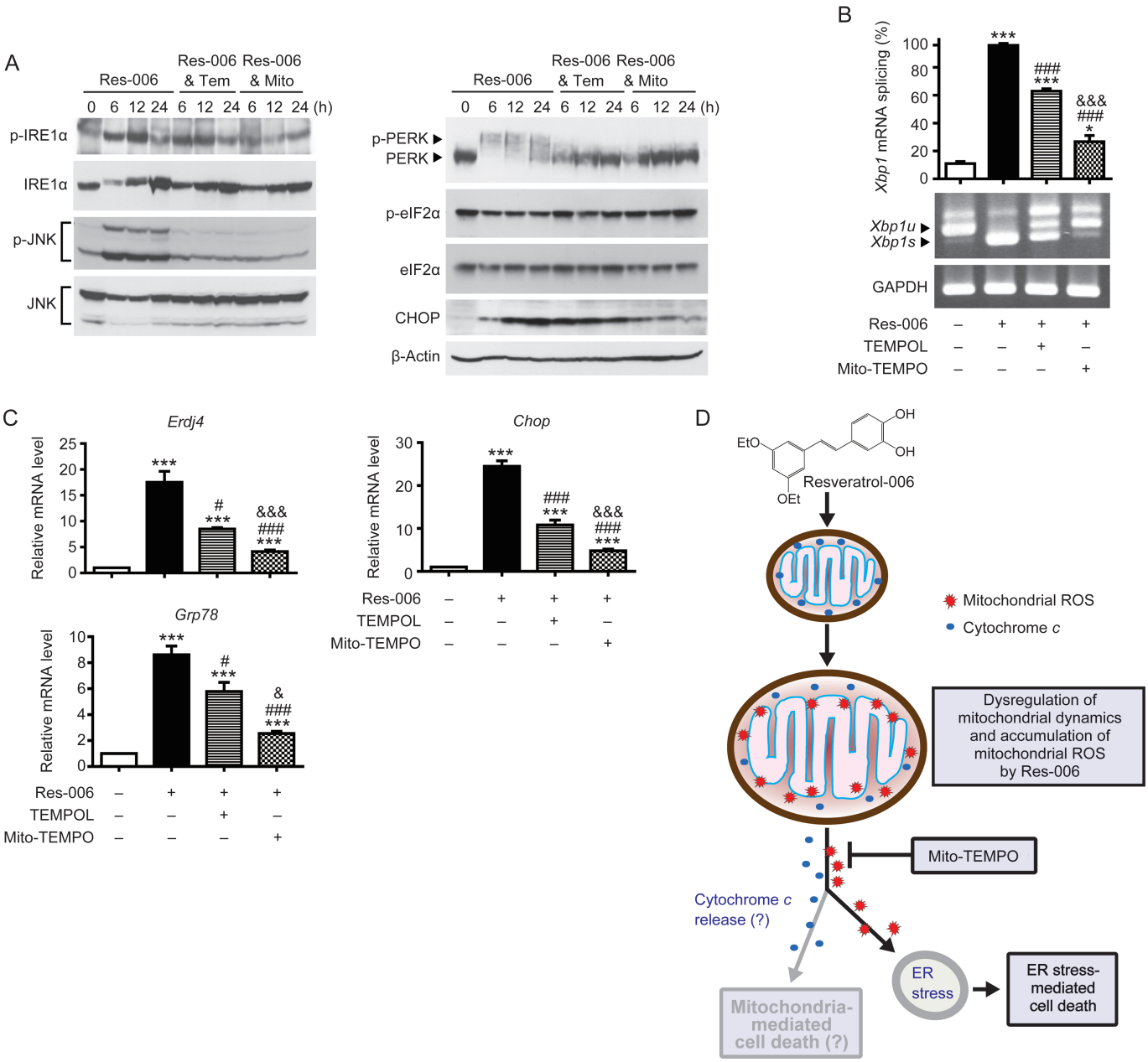

Figure 7. Res-006-mediated ER stress responses are strongly mitigated when mitochondrial-ROS accumulation is prevented. (A) HepG2 cells were treated with Res-006 (65 μmol/L) only, Res-006 (65 μmol/L) and Tempo (500 μmol/L), or Res-006 (65 μmol/L) and Mito-TEMPO (300 μmol/L) for the indicated times. Total cellular extracts were prepared and subjected to Western blot analysis. (B and C) HepG2 cells were treated with Res-006 (65 μmol/L) only, Res-006 (65 μmol/L) and Tempo (500 μmol/L), or Res-006 (65 μmol/L) and Mito-TEMPO (300 μmol/L) for 12 h. Total RNA was prepared and subjected to RT-PCR analysis (B) and qRT-PCR analysis (C). The data are expressed as the mean±SEM of three independent experiments, $^{*}P<0.05$ and $^{***}P<0.001$; untreated group *vs* each treated group, $^{\#}P<0.05$ and $^{\#\#\#}P<0.001$; Res-006-treated group *vs* each treated group, $^{\&}P<0.05$ and $^{\&\&\&}P<0.001$; Res-006- and TEMPOL-treated groups *vs* Res-006 and Mito-TEMPO-treated group. (D) Proposed cell death pathways induced by Res-006. Res-006 induces the dysregulation of mitochondrial dynamics and the accumulation of mitochondrial ROS in HepG2 cells. Mitochondrial ROS elicited ER stress and mediated cell death. The cytochrome c-mediated cell death pathway may be triggered by mitochondrial ROS accumulation. Res-006-induced cell death pathways can be blocked by the mitochondrial superoxide scavenger Mito-TEMPO.

In conclusion, our results demonstrate that cell death in human hepatoma HepG2 cells induced by the novel Res derivative, Res-006, is mediated by the activation of ER stress and the dysfunction of mitochondria that require ROS generation. The proposed cell death pathway induced by Res-006 is depicted in Figure 7D. The death involves cross-talk between the mitochondria and ER stress mechanisms. Our study provides a rationale for the development of a new resveratrol derivative as chemotherapeutic agent targeting both mitochondria and the ER.

Acknowledgements

This work was supported by the Basic Science Research Program (2011-0011433 and 2014R1A1A4A01004329), the Bio & Medical Technology Development Program (2012M3A9C3050632), and the Priority Research Centers Program (2014R1A6A1030318) of the National Research Foundation of Korea (NRF) funded by the Korean government.

Author contribution

Jae-woo PARK, Woo-gyun CHOI, Hyoungsu KIM, Hong-pyo KIM, and Sung-hoon BACK designed the research; Jae-woo PARK, Woo-gyun CHOI, Su-wol CHUNG, and Phil-jun LEE performed the experiments; Byung-sam KIM, Hun-taeg CHUNG, Sungchan CHO, Jong-heon KIM and Byoung-heon KANG contributed to the acquisition of the data; Jae-woo PARK, Woo-gyun CHOI, Phil-jun LEE, Hyoungsu KIM, Hong-pyo KIM, and Sung-hoon BACK analyzed and interpreted the data; Sung-hoon BACK wrote the draft manuscript, which was subsequently edited by all the authors, all of whom have read and approved the final manuscript.

Supplementary information

The supplementary information on the website of Acta Pharmacologica Sinica provides the confocal time-lapse movies of EYFP-labeled mitochondria in Mock- or Res-006-treated HepG2 cells, the MitoTracker Red-labeled mitochondria images of Res-006-treated THLE-2 and HepG2 cells, and the synthesis methods for Res-005 and Res-006.

References

1 Baur JA, Sinclair DA. Therapeutic potential of resveratrol: the *in vivo* evidence. Nat Rev Drug Discov 2006; 5: 493–506.
2 Ramprasath VR, Jones PJ. Anti-atherogenic effects of resveratrol. Eur J Clin Nutr 2010; 64: 660–8.
3 Athar M, Back JH, Kopelovich L, Bickers DR, Kim AL. Multiple molecular targets of resveratrol: Anti-carcinogenic mechanisms. Arch Biochem Biophys 2009; 486: 95–102.
4 Zupancic S, Lavric Z, Kristl J. Stability and solubility of *trans*-resveratrol are strongly influenced by pH and temperature. Eur J Pharm Biopharm 2015; 93: 196–204.
5 Walle T, Hsieh F, DeLegge MH, Oatis JE Jr, Walle UK. High absorption but very low bioavailability of oral resveratrol in humans. Drug Metab Dispos 2004; 32: 1377–82.
6 Rivera H, Shibayama M, Tsutsumi V, Perez-Alvarez V, Muriel P. Resveratrol and trimethylated resveratrol protect from acute liver damage induced by CCl_4 in the rat. J Appl Toxicol 2008; 28: 147–55.
7 Tabata Y, Takano K, Ito T, Iinuma M, Yoshimoto T, Miura H, *et al*. Vaticanol B, a resveratrol tetramer, regulates endoplasmic reticulum stress and inflammation. Am J Physiol Cell Physiol 2007; 293: C411–8.
8 Schneider Y, Chabert P, Stutzmann J, Coelho D, Fougerousse A, Gosse F, *et al*. Resveratrol analog (Z)-3,5,4'-trimethoxystilbene is a potent anti-mitotic drug inhibiting tubulin polymerization. Int J Cancer 2003; 107: 189–96.
9 Kroemer G, Galluzzi L, Brenner C. Mitochondrial membrane permeabilization in cell death. Physiol Rev 2007; 87: 99–163.
10 Lin X, Wu G, Huo WQ, Zhang Y, Jin FS. Resveratrol induces apoptosis associated with mitochondrial dysfunction in bladder carcinoma cells. Int J Urol 2012; 19: 757–64.
11 Sassi N, Mattarei A, Azzolini M, Szabo I, Paradisi C, Zoratti M, *et al*. Cytotoxicity of mitochondria-targeted resveratrol derivatives: interactions with respiratory chain complexes and ATP synthase. Biochim Biophys Acta 2014; 1837: 1781–9.
12 Mukherjee N, Parida PK, Santra A, Ghosh T, Dutta A, Jana K, *et al*. Oxidative stress plays major role in mediating apoptosis in filarial nematode *Setaria cervi* in the presence of *trans*-stilbene derivatives. Free Radic Biol Med 2016; 93: 130–44.
13 Ron D, Walter P. Signal integration in the endoplasmic reticulum unfolded protein response. Nat Rev Mol Cell Biol 2007; 8: 519–29.
14 Back SH, Kaufman RJ. Endoplasmic reticulum stress and type 2 diabetes. Annu Rev Biochem 2012; 81: 767–93.
15 Yoshida H, Matsui T, Yamamoto A, Okada T, Mori K. XBP1 mRNA is induced by ATF6 and spliced by IRE1 in response to ER stress to produce a highly active transcription factor. Cell 2001; 107: 881–91.
16 Wek RC, Cavener DR. Translational control and the unfolded protein response. Antioxid Redox Signal 2007; 9: 2357–71.
17 Harding HP, Novoa I, Zhang Y, Zeng H, Wek R, Schapira M, *et al*. Regulated translation initiation controls stress-induced gene expression in mammalian cells. Mol Cell 2000; 6: 1099–108.
18 Haze K, Yoshida H, Yanagi H, Yura T, Mori K. Mammalian transcription factor ATF6 is synthesized as a transmembrane protein and activated by proteolysis in response to endoplasmic reticulum stress. Mol Biol Cell 1999; 10: 3787–99.
19 Shen J, Prywes R. Dependence of site-2 protease cleavage of ATF6 on prior site-1 protease digestion is determined by the size of the luminal domain of ATF6. J Biol Chem 2004; 279: 43046–51.
20 Yamamoto K, Sato T, Matsui T, Sato M, Okada T, Yoshida H, *et al*. Transcriptional induction of mammalian ER quality control proteins is mediated by single or combined action of ATF6alpha and XBP1. Dev Cell 2007; 13: 365–76.
21 Wu J, Rutkowski DT, Dubois M, Swathirajan J, Saunders T, Wang J, *et al*. ATF6alpha optimizes long-term endoplasmic reticulum function to protect cells from chronic stress. Dev Cell 2007; 13: 351–64.
22 Harding HP, Zhang Y, Zeng H, Novoa I, Lu PD, Calfon M, *et al*. An integrated stress response regulates amino acid metabolism and resistance to oxidative stress. Mol Cell 2003; 11: 619–33.
23 Tabas I, Ron D. Integrating the mechanisms of apoptosis induced by endoplasmic reticulum stress. Nat Cell Biol 2011; 13: 184–90.
24 Kim I, Xu W, Reed JC. Cell death and endoplasmic reticulum stress: disease relevance and therapeutic opportunities. Nat Rev Drug Discov 2008; 7: 1013–30.
25 Urano F, Wang X, Bertolotti A, Zhang Y, Chung P, Harding HP, *et al*. Coupling of stress in the ER to activation of JNK protein kinases by transmembrane protein kinase IRE1. Science 2000; 287: 664–6.
26 Nishitoh H, Matsuzawa A, Tobiume K, Saegusa K, Takeda K, Inoue K, *et al*. ASK1 is essential for endoplasmic reticulum stress-induced neuronal cell death triggered by expanded polyglutamine repeats. Genes Dev 2002; 16: 1345–55.
27 Han D, Lerner AG, Vande Walle L, Upton JP, Xu W, Hagen A, *et al*. IRE1alpha kinase activation modes control alternate endoribonuclease outputs to determine divergent cell fates. Cell 2009; 138: 562–75.
28 Upton JP, Wang L, Han D, Wang ES, Huskey NE, Lim L, *et al*. IRE1alpha cleaves select microRNAs during ER stress to derepress translation of proapoptotic caspase-2. Science 2012; 338: 818–22.
29 Ma Y, Brewer JW, Diehl JA, Hendershot LM. Two distinct stress signaling pathways converge upon the CHOP promoter during the mammalian unfolded protein response. J Mol Biol 2002; 318: 1351–65.

30 Puthalakath H, O'Reilly LA, Gunn P, Lee L, Kelly PN, Huntington ND, *et al*. ER stress triggers apoptosis by activating BH3-only protein Bim. Cell 2007; 129: 1337–49.
31 McCullough KD, Martindale JL, Klotz LO, Aw TY, Holbrook NJ. Gadd153 sensitizes cells to endoplasmic reticulum stress by down-regulating Bcl-2 and perturbing the cellular redox state. Mol Cell Biol 2001; 21: 1249–59.
32 Park JW, Woo KJ, Lee JT, Lim JH, Lee TJ, Kim SH, *et al*. Resveratrol induces pro-apoptotic endoplasmic reticulum stress in human colon cancer cells. Oncol Rep 2007; 18: 1269–73.
33 Gwak H, Kim S, Dhanasekaran DN, Song YS. Resveratrol triggers ER stress-mediated apoptosis by disrupting N-linked glycosylation of proteins in ovarian cancer cells. Cancer Lett 2016; 371: 347–53.
34 Fan XX, Yao XJ, Xu SW, Wong VK, He JX, Ding J, *et al*. (Z)3,4,5,4'-*trans*-tetramethoxystilbene, a new analogue of resveratrol, inhibits gefitinb-resistant non-small cell lung cancer via selectively elevating intracellular calcium level. Sci Rep 2015; 5: 16348.
35 Jee MH, Hong KY, Park JH, Lee JS, Kim HS, Lee SH, *et al*. New mechanism of hepatic fibrogenesis: Hepatitis C virus infection induces transforming growth factor beta1 production through glucose-regulated protein 94. J Virol 2015; 90: 3044–55.
36 Back SH, Scheuner D, Han J, Song B, Ribick M, Wang J, *et al*. Translation attenuation through eIF2alpha phosphorylation prevents oxidative stress and maintains the differentiated state in beta cells. Cell Metab 2009; 10: 13–26.
37 Gu S, Chen C, Jiang X, Zhang Z. ROS-mediated endoplasmic reticulum stress and mitochondrial dysfunction underlie apoptosis induced by resveratrol and arsenic trioxide in A549 cells. Chem Biol Interact 2016; 245: 100–9.
38 Olden K, Pratt RM, Jaworski C, Yamada KM. Evidence for role of glycoprotein carbohydrates in membrane transport: specific inhibition by tunicamycin. Proc Natl Acad Sci U S A 1979; 76: 791–5.
39 Zhou L, Jiang L, Xu M, Liu Q, Gao N, Li P, *et al*. Miltirone exhibits antileukemic activity by ROS-mediated endoplasmic reticulum stress and mitochondrial dysfunction pathways. Sci Rep 2016; 6: 20585.
40 Boya P, Cohen I, Zamzami N, Vieira HL, Kroemer G. Endoplasmic reticulum stress-induced cell death requires mitochondrial membrane permeabilization. Cell Death Differ 2002; 9: 465–7.
41 Win S, Than TA, Fernandez-Checa JC, Kaplowitz N. JNK interaction with Sab mediates ER stress induced inhibition of mitochondrial respiration and cell death. Cell Death Dis 2014; 5: e989.
42 Orrenius S, Gogvadze V, Zhivotovsky B. Mitochondrial oxidative stress: implications for cell death. Annu Rev Pharmacol Toxicol 2007; 47: 143–83.
43 Murphy MP. How mitochondria produce reactive oxygen species. Biochem J 2009; 417: 1–13.
44 Madesh M, Hawkins BJ, Milovanova T, Bhanumathy CD, Joseph SK, Ramachandrarao SP, *et al*. Selective role for superoxide in InsP3 receptor-mediated mitochondrial dysfunction and endothelial apoptosis. J Cell Biol 2005; 170: 1079–90.
45 Galloway CA, Yoon Y. Perspectives on: SGP symposium on mitochondrial physiology and medicine: what comes first, misshape or dysfunction? The view from metabolic excess. J Gen Physiol 2012; 139: 455–63.
46 Tirasophon W, Welihinda AA, Kaufman RJ. A stress response pathway from the endoplasmic reticulum to the nucleus requires a novel bifunctional protein kinase/endoribonuclease (Ire1p) in mammalian cells. Genes Dev 1998; 12: 1812–24.
47 Calfon M, Zeng H, Urano F, Till JH, Hubbard SR, Harding HP, *et al*. IRE1 couples endoplasmic reticulum load to secretory capacity by processing the XBP-1 mRNA. Nature 2002; 415: 92–6.
48 Lee AH, Iwakoshi NN, Glimcher LH. XBP-1 regulates a subset of endoplasmic reticulum resident chaperone genes in the unfolded protein response. Mol Cell Biol 2003; 23: 7448–59.
49 Fawcett TW, Martindale JL, Guyton KZ, Hai T, Holbrook NJ. Complexes containing activating transcription factor (ATF)/cAMP-responsive-element-binding protein (CREB) interact with the CCAAT/enhancer-binding protein (C/EBP)-ATF composite site to regulate Gadd153 expression during the stress response. Biochem J 1999; 339: 135–41.
50 Palam LR, Baird TD, Wek RC. Phosphorylation of eIF2 facilitates ribosomal bypass of an inhibitory upstream ORF to enhance CHOP translation. J Biol Chem 2011; 286: 10939–49.
51 Willems PH, Rossignol R, Dieteren CE, Murphy MP, Koopman WJ. Redox homeostasis and mitochondrial dynamics. Cell Metab 2015; 22: 207–18.
52 Picard M, Shirihai OS, Gentil BJ, Burelle Y. Mitochondrial morphology transitions and functions: implications for retrograde signaling? Am J Physiol Regul Integr Comp Physiol 2013; 304: R393–406.
53 Gledhill JR, Montgomery MG, Leslie AG, Walker JE. Mechanism of inhibition of bovine F1-ATPase by resveratrol and related polyphenols. Proc Natl Acad Sci U S A 2007; 104: 13632–7.
54 Holtz WA, Turetzky JM, Jong YJ, O'Malley KL. Oxidative stress-triggered unfolded protein response is upstream of intrinsic cell death evoked by parkinsonian mimetics. J Neurochem 2006; 99: 54–69.
55 Kim SH, Kim KY, Yu SN, Seo YK, Chun SS, Yu HS, *et al*. Silibinin induces mitochondrial NOX4-mediated endoplasmic reticulum stress response and its subsequent apoptosis. BMC Cancer 2016; 16: 452.